Earth, Planets and Space
a SpringerOpen Journal

LETTER Open Access

The effect of heterogeneous crust on earthquakes: a case study of the 2004 Chuetsu, Japan earthquake

Takashi Miyatake

Abstract

The cause of asperities (i.e., high-slip regions) remains the subject of much debate in seismology. Several tomography studies have reported previously that high-velocity bodies coincide with asperities. However, it remains unclear whether the heterogeneity of the crust generates these asperities. This can be addressed by conducting stress analysis. The 2004 Chuetsu, Japan earthquake is one of the best examples, since a detailed 3D seismic velocity structure was elucidated. For the resulting structural model, we calculated the heterogeneous stress distribution numerically, adding tectonic loading. Then, we calculated the distribution of the stress drop on the fault based on a frictional coefficient μ_d, the pore fluid factor λ_v, and the tectonic loading ratio c. We assumed λ_v to be 0.85 based on a previous study and calculated the corresponding slip distributions and seismic moment. To have been responsible for this Mw6.6 earthquake, the parameters μ_d and c must have been located somewhere along a particular line in $c - \mu_d$ space; this constrains the possible range of these parameters. We found that the asperity region for the above slip distribution corresponds approximately to that of the kinematic model, which suggests that the asperity may have been created by heterogeneity in the crustal structure.

Findings

The causes of asperities or high-slip areas on faults remain unclear. An asperity was defined originally as the protrusion of a frictional surface in rock mechanics and an asperity model was proposed to explain various types of seismicity along plate boundaries (Kanamori 1981). In this model, asperities are represented as regions of high strength and can accumulate high stress (Das and Kostrov 1983; Lay and Kanamori 1981). Conversely, asperities are often considered to be regions of high slip (e.g., Somerville et al. 1999). In the present study, we adopt the latter definition and omit any discussion of strength. Regardless of the particular meaning preferred, it is generally believed that fault processes (and thus asperities) are controlled by the frictional properties on faults. The inherent variability of fault's frictional properties has allowed the emergence of a wide variety of fault rupture processes; yet coincidence between asperities and bodies with high seismic velocity has been reported previously for several source regions (Michael and Eberhart-Phillips 1991; Chiarabba and Amato 2003; Kato et al. 2010), suggesting that the stress field itself may cause asperities. However, it remains unclear whether the frictional properties of fault surfaces or stress field characteristics are the primary factors controlling the development of asperities. In the present study, we attempt to address this gap in knowledge by investigating the effects of the stress field on asperities. The 2004 Chuetsu earthquake in Japan and its source region provide an excellent case study in this regard. The highly resolved velocity structure of this earthquake has been inferred from the arrival times of aftershocks, observed by an extremely dense network of temporary seismic stations (Kato et al. 2006, 2009) that detected the presence of a high-velocity body that coincided approximately with an asperity (Kato et al. 2010). For this heterogeneous structural model, we calculate the heterogeneous stress distribution on the fault numerically using the finite difference method (FDM). If the asperity (i.e., high-slip region) can be shown to have been created

Correspondence: miyatake@eri.u-tokyo.ac.jp
Earthquake Research Institute, The University of Tokyo, 1-1-1 Yayoi, Bunkyo, Tokyo 113-0032, Japan

by the stress field in our stress analysis, it can be considered likely that the asperity was caused by this heterogeneous stress field generated by a heterogeneous crustal structure.

Stress on the fault

We assumed that the stress on the fault consisted of two parts: tectonic loading stress $\sigma_{ij}^{\text{System}-1}$ (hereafter, system-1) and lithostatic stress $\sigma_{ij}^{\text{System}-2}$ (hereafter, system-2). Accordingly, the total stress can be defined as follows:

$$\sigma_{ij} = \sigma_{ij}^{\text{System}-1} + \sigma_{ij}^{\text{System}-2}. \tag{1}$$

In the stress computation for system-1, we extracted a modeling space of 100 km × 100 km × 50 km (Figure 1) and included the source area of the 2004 Chuetsu earthquake. The *X*-, *Y*-, and *Z*-axes were the same as those of Kato et al. (2006), except that the horizontal origin was the fault center. The *Y*-axis corresponded to the fault strike of the mainshock, whereas the *Z*-axis is taken to be upward.

We solved the elastic equilibrium equations and stress–strain relationships represented by Equations 2 and 3, respectively:

$$\begin{aligned}
\frac{\partial \sigma_{xx}}{\partial x} + \frac{\partial \sigma_{xy}}{\partial y} + \frac{\partial \sigma_{xz}}{\partial z} &= 0 \\
\frac{\partial \sigma_{yx}}{\partial x} + \frac{\partial \sigma_{yy}}{\partial y} + \frac{\partial \sigma_{yz}}{\partial z} &= 0 \\
\frac{\partial \sigma_{zx}}{\partial x} + \frac{\partial \sigma_{zy}}{\partial y} + \frac{\partial \sigma_{zz}}{\partial z} &= 0
\end{aligned} \tag{2}$$

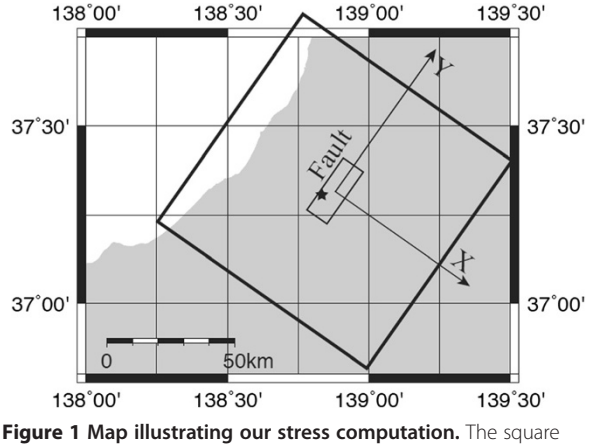

Figure 1 Map illustrating our stress computation. The square depicts the computational space. The star indicates the epicenter of the event.

$$\begin{aligned}
\sigma_{xx} &= (\lambda + 2\mu)\frac{\partial u_x}{\partial x} + \lambda \frac{\partial u_y}{\partial y} + \lambda \frac{\partial u_z}{\partial z} \\
\sigma_{yy} &= \lambda \frac{\partial u_x}{\partial x} + (\lambda + 2\mu)\frac{\partial u_y}{\partial y} + \lambda \frac{\partial u_z}{\partial z} \\
\sigma_{zz} &= \lambda \frac{\partial u_x}{\partial x} + \lambda \frac{\partial u_y}{\partial y} + (\lambda + 2\mu)\frac{\partial u_z}{\partial z}
\end{aligned} \tag{3}$$

$$\begin{aligned}
\sigma_{xy} &= \mu\left(\frac{\partial u_x}{\partial y} + \frac{\partial u_y}{\partial x}\right) \\
\sigma_{yz} &= \mu\left(\frac{\partial u_y}{\partial z} + \frac{\partial u_z}{\partial y}\right) \\
\sigma_{zx} &= \mu\left(\frac{\partial u_x}{\partial z} + \frac{\partial u_z}{\partial x}\right)
\end{aligned}$$

where λ and μ represent Lamé constants whose distributions were obtained using a previously developed 3D velocity model (Kato et al. 2006) and from the relationship between P wave velocity and density (Birch 1961), respectively.

The following boundary conditions were also imposed (see also A' in Appendix A):

$$\begin{aligned}
&u_x(L_x, y, z) = -u_0 \\
&u_x(-L_x, y, z) = u_0 \\
&\sigma_{xy}(L_x, y, z) = \sigma_{xy}(-L_x, y, z) = 0 \\
&\sigma_{zx}(L_x, y, z) = \sigma_{zx}(-L_x, y, z) = 0 \\
&\sigma_{xy}\left(x, L_y, z\right) = \sigma_{xy}\left(x, -L_y, z\right) = 0 \\
&\sigma_{yz}\left(x, L_y, z\right) = \sigma_{yz}\left(x, -L_y, z\right) = 0 \\
&\sigma_{yy}\left(x, L_y, z\right) = \sigma_{yy}\left(x, -L_y, z\right) = 0 \\
&\sigma_{zx}(x, y, 0) = \sigma_{zx}(x, y, -L_z) = 0 \\
&\sigma_{yz}(x, y, 0) = \sigma_{yz}(x, y, -L_z) = 0 \\
&\sigma_{zz}(x, y, 0) = \sigma_{zz}(x, y, -L_z) = 0
\end{aligned} \tag{4}$$

In our computation, $L_x = L_y = L_z = 50$ km. The displacement u_0 in Equation 4 may relate to a plate motion. Because the absolute value of the boundary condition (i.e., u_0) in Equation 4 was not known, we tentatively assumed $u_0 = u_0^0$, where $u_0^0/(2L_z) = 10^{-5}$. Moreover, the resultant stress field $\sigma_{ij}^{\prime}$Tectonic had to be adjusted by multiplying with a constant, c ($= u_0/u_0^0$).

Therefore,

$$\sigma_{ij}^{\text{System}-1} = c\sigma_{ij}^{\prime\text{Tectonic}}. \tag{5}$$

We obtained the stress field for $c = 1$ using the FDM in which grid sizes are taken as 0.4 km for *z*-axis and 0.3 km for horizontal axes. This ratio corresponded approximately to the dip angle of the fault. We also applied the successive over-relaxation (SOR) iterative method (Press et al. 1992) in our computation.

The calculated stress distributions and the rigidity of the fault are illustrated in Figure 2. The ratio of fault shear to the normal stress component on the fault is also shown in Figure 2d. Because $\sigma/\sigma_n = \tau_s/\sigma_n - \mu_d$, this shear/normal stress ratio can indicate stress drop, where σ is

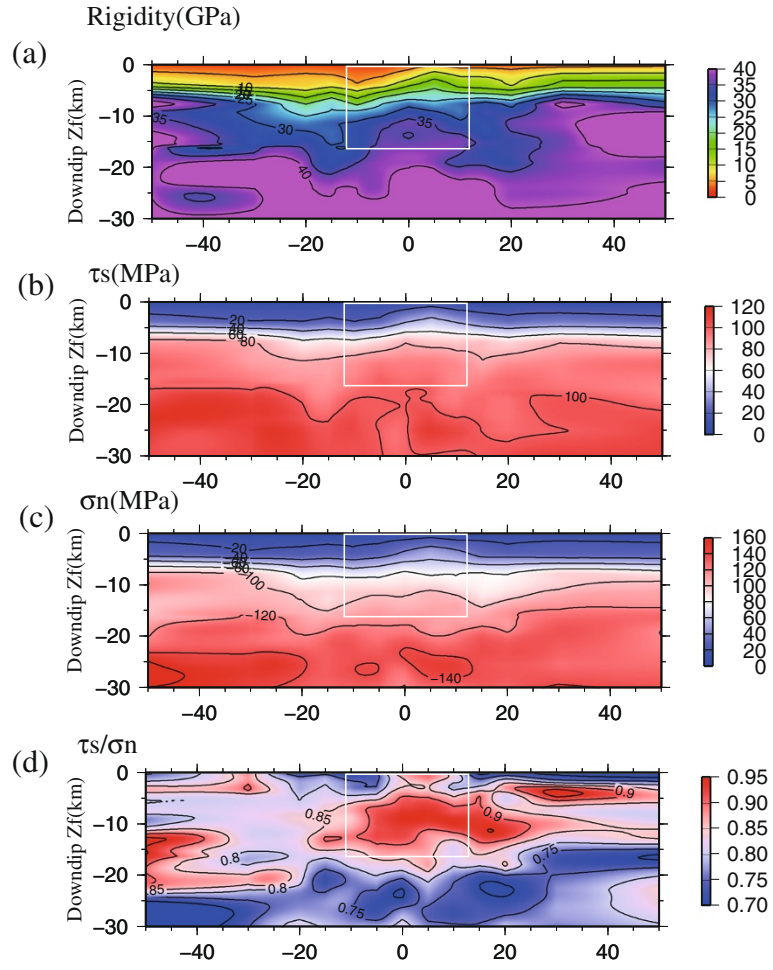

Figure 2 Calculated stress distributions and the rigidity on the fault. (a) Rigidity distribution on the mainshock fault with a contour interval of 2 GPa. **(b)** Computed shear stress components τ_s on the fault. **(c)** Normal stress τ_n. **(d)** τ_s/τ_n. The white square indicates the mainshock fault (Hikima and Koketsu 2005).

stress drop and μ_d is a dynamic frictional coefficient. In the present study, we assumed μ_d to be uniform. It should be noted that the above fault normal stress is taken to be a positive value for compression, whereas σ_{xx}, σ_{yy}, and σ_{zz} are positive for tension. The figure suggests that the heterogeneous crust resulted in a large stress drop around the 2004 Chuetsu earthquake. Two other areas of high shear/normal stress ratios are apparent in Figure 2d. However, one of these occurs around the shallower part from $x = 20$ to 40 km which might have very small stress drop; the other is located at a depth of around 15 km and corresponds to $x < -40$ km, which is too deep to be associated with the 2004 Chuetsu earthquake. Therefore, we computed the stresses on a region with a length twice that of the fault associated with the 2004 Chuetsu earthquake.

In system-2, we considered both lithostatic stress and fluid pressure. Thus, $\sigma_{xx} = \sigma_{yy} = \sigma_{zz} = \sigma_V = \rho g z$, where ρ, g, and z are density, gravitational acceleration, and depth, respectively.

Finally, the total stress was calculated as follows:

$$\sigma_{ij} = c\sigma_{ij}^{'\mathrm{Tectonic}} + \sigma_{ij}^{\mathrm{Lithostatic}}. \tag{6}$$

For a given value of parameter c, the stress on the fault was determined completely. Given the values for the dynamic frictional coefficient (μ_d), a pore fluid factor (λ_v), and a constant c, the stress drop $\Delta\sigma(\xi, \eta; c, \mu_d, \lambda_V)$ at (ξ, η) on the fault was calculated as follows:

$$\Delta\sigma(\xi,\eta;c,\mu_d,\lambda_V) = c\tau_s(\xi,\eta) - \mu_d[c\sigma_n(\xi,\eta) + (1-\lambda_V)\sigma_V(\xi,\eta)] \tag{7}$$

It should be noted that the above stress drop is not a true stress drop; rather, it is a potential value based on the assumption that the rupture occurred along the entire region

of positive stress drop on the fault. Therefore, this can be considered an approximation of the stress drop that can be used as an initial model for dynamic rupture simulation.

Slip distributions

The stress drop distribution described above is controlled by the tectonic loading imposed by the heterogeneity of the crustal structure. To ascertain whether such a stress drop could have generated the mainshock of the 2004 Chuetsu earthquake, we calculated the slip distribution due to the stress drop distribution, described in Equation 7, and compared it with the kinematic model slip distribution (Hikima and Koketsu 2005). Three primary parameters are required (either given or assumed) to calculate the stress drop and estimate the slip distribution according to Equation 7: μ_d, c, and λ_v. However, the computation of the slip distribution due to stress drop on a fault in a heterogeneous structure is extremely time-consuming because it requires more than several thousand computations to constrain the parameters.

To address this, we simply estimated the slip distribution caused by the stress drop $\sigma(\xi, \eta; c, \mu_d, \lambda_V)$ by solving the following equation:

$$\Delta\sigma(x,y) = \iint G(x,y;\xi,\eta)\Delta u(\xi,\eta)d\xi d\eta \tag{8}$$

where $G(x, y; \xi, \eta)$ is a Green's function for a uniform half space. Then, we discretized Equation (8):

$$\begin{pmatrix} \Delta\sigma_1 \\ \Delta\sigma_2 \\ \\ \Delta\sigma_M \end{pmatrix} = \begin{pmatrix} G_{11} & G_{12} & & G_{1M} \\ G_{21} & G_{22} & & G_{2M} \\ & & & \\ G_{M1} & G_{M2} & & G_{MM} \end{pmatrix} \begin{pmatrix} \Delta u_1 \\ \Delta u_2 \\ \\ \Delta u_M \end{pmatrix} \tag{9}$$

where Δu_L and $\Delta\sigma_L$ are slip and shear stress drop at fault element L of (ξ_i, η_j). L is given by $L = i + (j - 1)\ M$, where $i = 1,\ldots, M$ and $j = 1,\ldots, N$. To reduce computation time, we calculated the slip on the size of the twice longer fault than the kinematic model. For a given shear stress drop distribution $\Delta\sigma_L$, we were able to solve the slip distribution Δu_L. In this computation, we assumed that $Vp = 5.5\,\mathrm{km/s}$, $Vs = Vp/\sqrt{3}$, and $\rho = 2.8\ \mathrm{g/cm^3}$ and used the code of Okada (1992) for computation of *Gij*. The differences in slip distribution between our method and the heterogeneous model are presented in Appendix B.

Although Equation 7 can be used to calculate stress drop distributions on the fault, it has three unknown parameters (c, μ_d, and λ_v). Of these, λ_v was estimated by Sibson (2007) to be 0.75 to 0.95 for our study region. Accordingly, we tentatively assumed $\lambda_v = 0.85$ in the present study. We calculated slip distributions for a region of 50 km × 16 km (i.e., two times longer than the mainshock) and varied c and μ_d as follows: between 0.001 and 5.0 in increments of 0.001 for c and between 0.001 and 1.0 in increments of 0.001 for μ_d. In total, we calculated 500 × 1,000 slip distributions. We also calculated seismic moments and plotted their distribution (Figure 3). The results demonstrate that for a given absolute stress parameter c, a low dynamic frictional coefficient resulted in high stress, large slip, and high seismic moment. We also obtained the conditions for an earthquake with a seismic moment of 8.8×10^{18} Nm (Hikima and Koketsu 2005) and have plotted as a white line in Figure 3.

The slip distributions for several pairs of μ_d and c values that plotted along the white line in Figure 3 are presented in Figure 4. It is clear that the lower values of c tend to generate broader asperities in areas with less heterogeneous stress distribution. Conversely, higher c values produced more concentrated slip. In all cases, the asperity occurred at almost the same location as in the kinematic model (see bottom right of Figure 4), although the asperity simulated according to our method was found to be slightly shallower than that of the kinematic model. Furthermore, our asperity corresponds to an area of high shear/normal stress ratio that can be shown in Figure 2.

Discussion

As Sibson (2007) estimated λ_v to be between 0.75 and 0.95 for our study region, we assumed a constant λ_v of 0.85. Typically, lower values of λ_v correspond to a requirement for higher loading stress, which corresponds to higher values of c. Through additional computations, we found c to increase by about 30% for a given value of μ_d when we set $\lambda_v = 0.8$, although the stress drop distribution was found to be very similar to that for $\lambda_v = 0.85$.

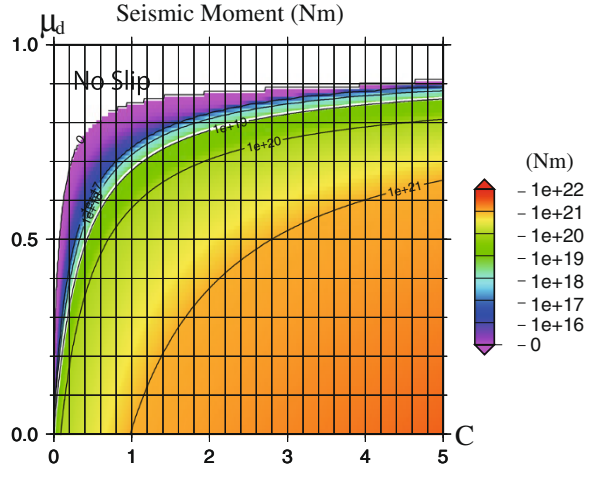

Figure 3 Seismic moment for c and the dynamic frictional coefficient μ_d. The white line indicates seismic moment of 8.8×10^{18} Nm, which is same as that of the Chuetsu earthquake (Hikima and Koketsu 2005).

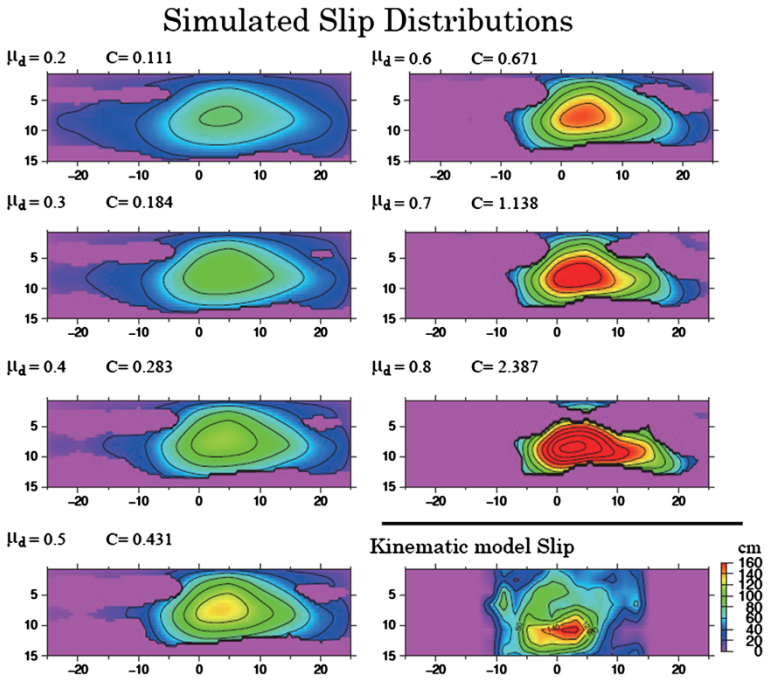

Figure 4 Slip distributions for selected pairs of *c* and μ_d values along the white line in Figure 3. Kinematic model slip distribution is shown at the bottom right.

Thus, it is clear that the value of λ_v does not affect the overall distribution of the stress drop, although heterogeneity of λ_v may have some effect on stress distribution. Heterogeneous distributions of λ_v have not been reported extensively, although Terakawa and Miller (2012) tried to estimate the regional variation in pore fluid pressure in Basel, Switzerland, using Centroid Moment Tensor (CMT) inversion results based on the assumption that tectonic stress is uniform. Both the heterogeneity of fluid pressure and structure are known to be important for earthquake rupture. However, based on the coincidence of the asperity and the zone of high seismic velocity in the present study, the main features of the particular event studied here (e.g., the size and location of the asperity) appear to have been controlled primarily by the heterogeneous seismic velocity structure.

Shibazaki et al. (2008) used finite element analysis to demonstrate that the loading processes of large inland earthquakes in northeastern Japan are determined by the nonuniform thermal structure of the deeper crust and uppermost mantle. However, it has been demonstrated that coincidence between an asperity and high elastic properties (i.e., a high-seismic-velocity structure) cannot always be attributed to rheological properties. An asperity is a region of high moment release, which typically corresponds to large stress drop or high stress; thus, asperities can support strain energy. Therefore, the heterogeneity of elastic properties in the upper crust may create the initial conditions required for a given event, thus controlling the faulting process (i.e., the size and stress drop of asperities). Accordingly, we considered only the elasticity in our stress analysis.

We compared the slip distribution caused by crustal heterogeneity with that indicated by a previously developed kinematic slip model. Our crustal heterogeneity data were inverted using the DD tomography method (Zhang and Thurber 2003) and utilizing a huge dataset of aftershock arrival times observed by the dense seismic network deployed after the mainshock of the 2004 Chuetsu earthquake. Conversely, the kinematic model was inverted from the permanently strong ground motion station. Thus, the small offset (i.e., a few kilometers) between the asperity and the high-velocity body may have resulted from differences in the datasets and modeling parameters used or from differences in inversion method.

Conclusions

We investigated the effects of heterogeneous crustal structure on earthquake rupture, using the 2004 Chuetsu earthquake and its source region as a case study. In particular, we calculated the stress distribution numerically using a 3D crustal structure model of the source region. A region exhibiting a high ratio of shear to normal stress, which can be considered as an indicator of stress drop, was found to coincide approximately to the fault area of the 2004 Chuetsu earthquake. Then, we assumed values for several unknown parameters

(frictional coefficient μ_d, pore fluid factor λ_v, tectonic loading ratio c) to estimate the potential stress drop distribution. Using the grid search technique, we obtained the relationship between c and μ_d for the occurrence of an earthquake with a seismic moment of 8.8×10^{18} Nm. Under these conditions, we were able to reproduce the localized rupture area at a location that almost coincides with that of the asperity of the 2004 Chuetsu earthquake, suggesting that the asperity of the mainshock of this earthquake could have been created by a heterogeneous stress field generated from heterogeneous crustal structure. Overall, our results demonstrate that although the dynamic rupture of this asperity is controlled by the frictional properties of the fault surface, the stress field is also an important factor in asperity creation.

Appendix A

Boundary conditions

Because the studied event occurred as an almost pure thrust earthquake, the driving stress system is expected to have been as shown in Figure 5a. In this figure σ_z is assumed to the lithostatic pressure σ_V (=ρgz). After subtracting σ_V from σ_X, σ_Y, and σ_Z, the tectonic stress can be decomposed into two systems (Figure 5b): A and B. The functional forms of the tectonic stress σ_X and σ_Y are unknown. It should be noted that stress in Figure 5b and c are tectonic stress. The assumption that that σ_X is uniform in system A causes almost uniform shear and normal stresses on the fault. Strength (peak stress) and dynamic friction can be estimated when σ_V (=ρgz) is added to the fault normal stress, and the resultant normal stress is multiplied by static and dynamic frictional coefficients. Under these conditions, we found large stress drop in the shallower parts and minimum strength excess at the free surface. This suggests that the earthquake rupture must have started at the surface and that the stress drop must have been highest at the ground surface. These results can be avoided if the stress σ_X is assumed to increase with depth. The depth dependency is related to variations in elastic constants. The stress field in this region likely originated primarily from plate motions. Therefore, we selected the displacement boundary condition $u_X = u_0$, which corresponds to system A' in Figure 5c. It should be noted that other displacement components were not fixed, but free stress conditions (except the σ_{xx} component) were imposed according to Equation 4. After solving the stress field imposing the above boundary condition, the resultant stress component σ_{xx} was added on the boundary of $x = \pm L_X$ as a further boundary condition. The solution is the same as the problem in which the boundary condition of Equation 4 is imposed. Taking the linear elasticity into account, the target solution can be estimated by superposing solutions A and B in Figure 5b. System A is equivalent to system A'. The effect of system B on fault normal and shear stress is expected to be negligible, because these stresses are exactly zero for uniform structure. We estimated such effects in a heterogeneous structure by assuming that the value of $\sigma_Y = \sigma_{yy}(z)$ on the boundary of $y = \pm L_y$ is the same as $\sigma_{xx}(z)$ on the boundary

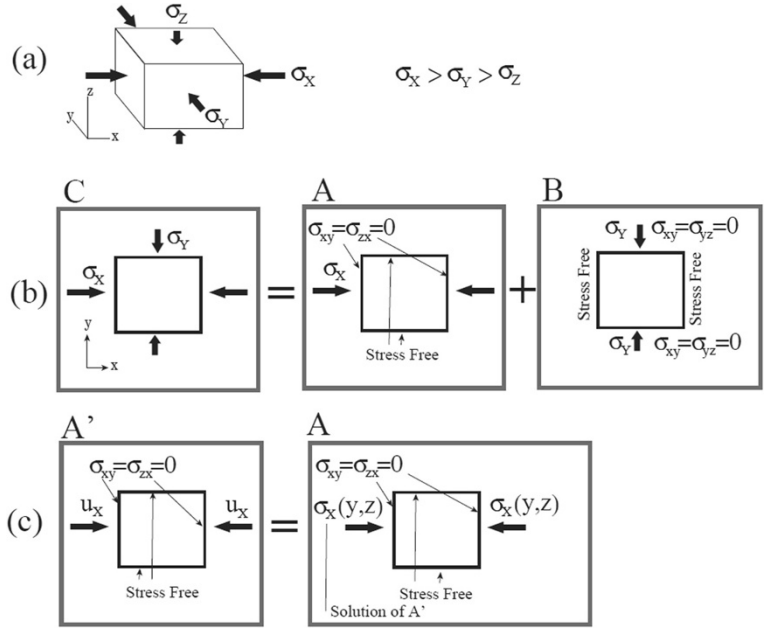

Figure 5 The systems A, B, and C. (a) Stress system for a thrust earthquake. **(b)** The system C is decomposed into B and C. **(c)** System A' is equivalent to system A, where $\sigma_x(y, z)$ is a solution of system A on the boundaries.

of $x = \pm L_x$. We found system B to exert little effect (less than 5%) on the stress components of σ_{zx}, σ_{xx}, and σ_{zz}. Thus, B had little effect on fault normal and shear stress on the fault plane, where $\sigma_{xx}(z)$ is the averaged stress component along the y-axis on the corresponding boundaries. Based on the condition of thrust earthquake that $|\sigma_X| > |\sigma_Y| > |\sigma_Z|$ (Figure 5a), we believed the abovementioned σ_{zx}, σ_{xx}, and σ_{zz} were overestimated in our study. Thus, we ignored the effects of system B.

Appendix B

The effects of heterogeneous crust on slip distribution

The effects of heterogeneous crust on fault slip for the Chuetsu region were investigated simply. Considering the stress drop $\Delta\sigma$ in our event, we assumed that $\Delta\sigma = 5$ MPa for $6.5 < Zf < 12.5$ and $\Delta\sigma = 1$ MPa for $0.5 < Zf < 6.5$ km (Figure 6). In the case of the heterogeneous crustal model, the slip distribution was calculated using the finite difference method (Kato et al. 2010) for a

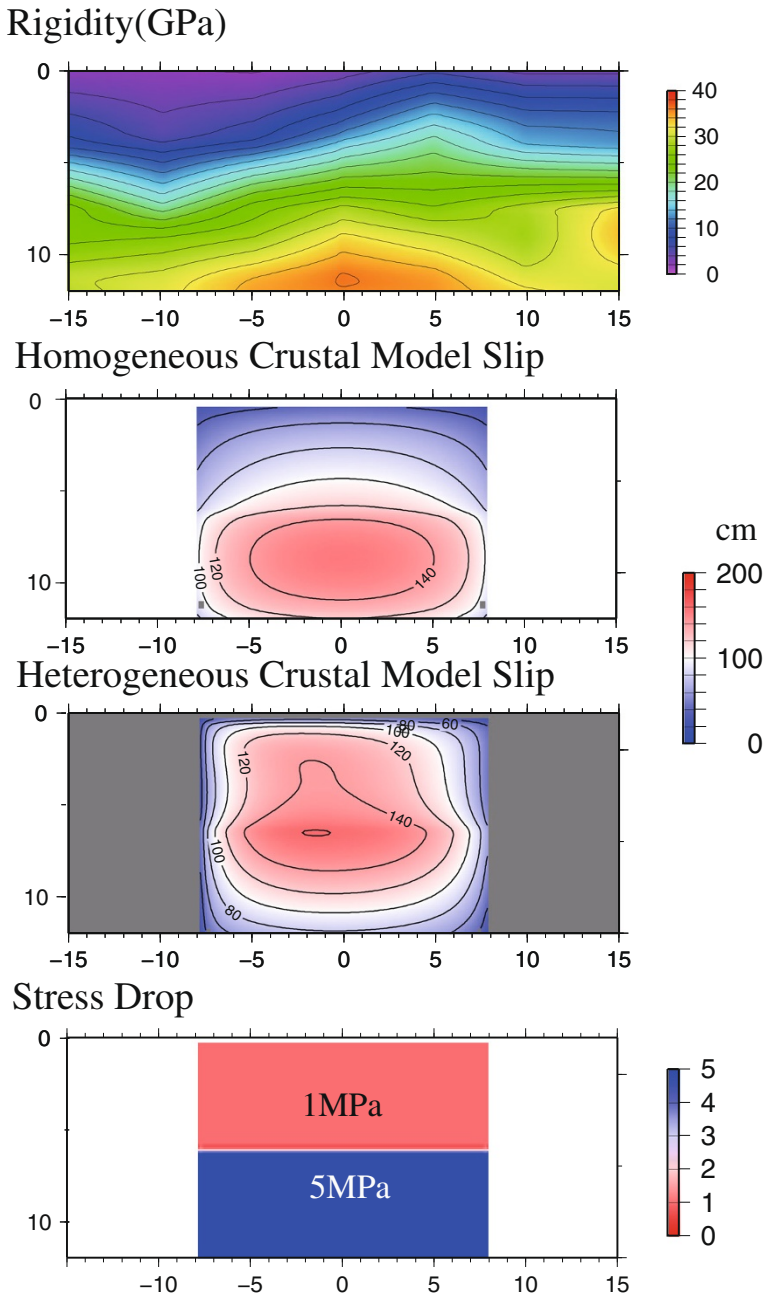

Figure 6 Comparison between slip distributions estimated using code of Okada and using the finite difference method. The distributions of rigidity and assumed stress drop are also plotted.

computational space of 60 km × 60 km × 60 km, although Figure 6 shows only the fault region. It is clear that the resultant slip distribution around the area of low rigidity has amplified the slip. Conversely, the fitting of slip distribution for the deeper parts of the crust (i.e., approximately 5 to 10 km) is satisfactory. Considering the asperity of the earthquake, the effects would be negligible in our case study.

Competing interest
The author declares that he has no competing interest.

Acknowledgements
The computations were conducted by the parallel computer of the Earthquake Information Center in the Earthquake Research Institute, University of Tokyo. I thank Dr. K. Hikima and Dr. A. Kato for providing their inversion data. I thank Dr. Shibazaki for valuable comments. I also acknowledge two anonymous reviews for helpful comments.

Received: 7 August 2013 Accepted: 26 November 2013
Published: 24 April 2014

References

Birch F (1961) The velocity of compressional waves in rocks to 10 kilobars, part 2. J Geophys Res 66:2199–2224
Chiarabba C, Amato A (2003) Vp and Vp/Vs images in the Mw 6.0 Colfiorito fault region (central Italy): a contribution to the understanding of seismotectonic and seismogenic processes. J Geophys Res 108:2248
Das S, Kostrov BV (1983) Breaking of a single asperity: rupture process and seismic radiation. J Geophys Res 88:4177–4288
Hikima K, Koketsu K (2005) Rupture processes of the 2004 Chuetsu (mid-Niigata prefecture) earthquake, Japan: a series of events in a complex fault system. Geophys Res Lett 32, L18303, doi:10.1029/2005GL023588
Kanamori H (1981) The nature of seismicity before large earthquakes. In: Ewing M, Simpson D, Richards P (eds) Earthquake prediction, an international review, 4th edn. American Geophysical Union, Washington DC, pp 1–19
Kato A, Sakai S, Hirata N, Kurashimo E, Iidaka T, Iwasaki T, Kanazawa T (2006) Imaging the seismic structure and stress field in the source region of the 2004 mid-Niigata Prefecture earthquake: structural zones of weakness and seismogenic stress concentration by ductile flow. J Geophys Res 111, B08308, doi:10.1029/2005JB004016
Kato A, Kurashimo E, Igarashi T, Sakai S, Iidaka T, Shinohara M, Kanazawa T, Yamada T, Hirata N, Iwasaki T (2009) Reactivation of ancient rift systems triggers devastating intraplate earthquakes. Geophys Res Lett 36, L05301, doi:10.1029/2008GL036450
Kato A, Miyatake T, Hirata N (2010) Asperity and barriers of the 2004 Mid-Niigata Prefecture earthquake revealed by highly dense seismic observations. Bull Seism Soc Am 100:298–306, doi:10.1785/0120090218
Lay T, Kanamori H (1981) An asperity model of large earthquake sequences. In: Ewing M, Simpson D, Richards P (eds) Earthquake prediction, an international review, 4th edn. American Geophysical Union, pp 579–592
Michael AJ, Eberhart-Phillips D (1991) Relations among fault behavior, subsurface geology, and three dimensional velocity models. Science 253:651–654
Okada Y (1992) Internal deformation due to shear and tensile faults in a half-space. Bull Seis Soc Am 82:1018–1040
Press WH, Teukolsky SA, Vetterling WT, Flannery BP (1992) Numerical recipes in FORTRAN, 2nd edn. Cambridge University Press, Cambridge, UK
Shibazaki B, Garatani K, Iwasaki T, Tanaka A, Iio Y (2008) Faulting processes controlled by the nonuniform thermal structure of the crust and uppermost mantle beneath the northeastern Japanese island arc. J Geophys Res 113, B08415, doi:10.1029/2007JB005361
Sibson RH (2007) An episode of fault-valve behaviour during compressional inversion?—The 2004 MJ6.8 Mid-Niigata Prefecture, Japan, earthquake sequence. Earth Planet Sci Letts 257:188–199
Somerville P, Irikura K, Graves R, Sawada S, Wald D, Abrahamson N, Iwasaki Y, Kagawa T, Smith N, Kowada A (1999) Characterizing crustal earthquake slip models for the prediction of strong ground motion. Seism Res Lett 70:59–80
Terakawa T, Miller SA, Deichmann N (2012) High fluid pressure and triggered earthquakes in the enhanced geothermal system in Basel, Switzerland. J Geophys Res 117, B07305, doi:10.1029/2011JB0089802012
Zhang H, Thurber CH (2003) Double-difference tomography: the method and its application to the Hayward fault, California. Bull Seismol Soc Am 93:1875–1889

doi:10.1186/1880-5981-66-18
Cite this article as: Miyatake: **The effect of heterogeneous crust on earthquakes: a case study of the 2004 Chuetsu, Japan earthquake.** *Earth, Planets and Space* 2014 **66**:18.